CDF note 9226
version 4

Public Note for: Search for Flavor-Changing Neutral Current $D^0 \to \mu^+\mu^-$ Decays Using 360 pb^{-1} of CDF Run II Data

The CDF Collaboration
URL http://www-cdf.fnal.gov
(2 March 2008)
(Updated 15 September 2010)

Abstract

We present an updated search for FCNC $D^0 \to \mu^+\mu^-$ decays using 360 pb^{-1} of Run II data. In addition to analyzing more data, the muon coverage is increased by also utilizing the CMX detector. The main source of background in the signal region is identified as coming from $B \to \mu^+\mu^- X$ decays. A probability ratio is used to optimize the analysis by reducing the dominant background, while keeping the signal region blinded. The analysis sensitivity at the 90% (95%) confidence level is 5.2×10^{-7} (6.0×10^{-7}).

The blind analysis expects a total of 8.7 ± 1.7 events, of which 4.9 ± 1.3 are expected in the CMU-CMU, 2.7 ± 1.0 in the CMU-CMX, and 1.0 ± 0.5 are expected in the CMX-CMX channels. After unblinding the data, 3 events are found in the CMU-CMU, no events in the CMU-CMX, and one event in the CMX-CMX channel. We use a hybrid frequentist/Bayesian approach to extract the 90% and 95% confidence level limits or belts on the branching fraction. The technique allows for the combination of several channels and the inclusion of nuisance parameters. We find $\mathcal{B}(D^0 \to \mu^+\mu^-) < 2.1 \times 10^{-7}$ (3.0×10^{-7}) at the 90% (95%) confidence level.

1 Introduction

In the Standard Model, the flavor-changing neutral current decay $D^0 \to \mu^+\mu^-$ is suppressed by the GIM mechanism. Figure 1 shows some of the basic Feynman diagrams contributing to $D^0 \to \mu^+\mu^-$ decays in the Standard Model. The decay rate is dominated by long-range contributions [1], in particular the diagram shown in Figure 2. The total Standard Model branching fraction is estimated [1] to be $\mathcal{B}(D^0 \to \mu^+\mu^-) \approx 4 \times 10^{-13}$.

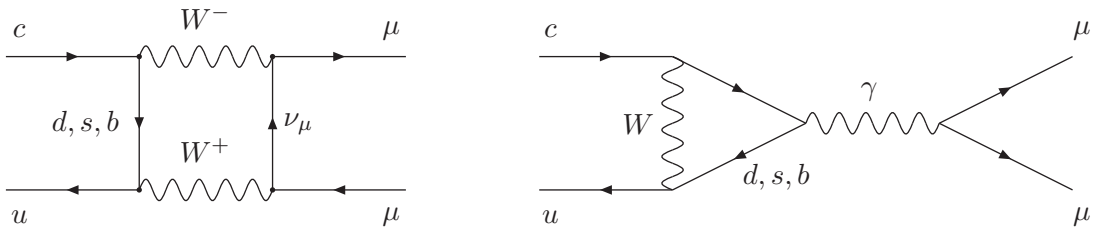

Figure 1: A few of the possible Feynman diagrams for the $D^0 \to \mu^+\mu^-$ decay in the Standard Model.

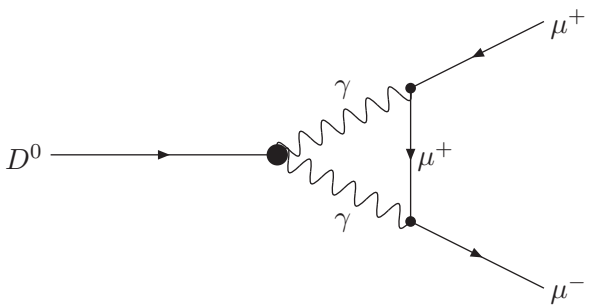

Figure 2: The dominant long-distance Feynman diagram for the $D^0 \to \mu^+\mu^-$ decay in the Standard Model

As opposed to $B_s^0 \to \mu^+\mu^-$, which is enhanced in SUSY models by $\tan\beta$ terms due to couplings with down-type quarks, virtually no enhancement of this decay is expected from the canonical, $\mathcal{R}$-parity conserving SUSY models. However, in $\mathcal{R}$-parity violating SUSY models, enhancements are possible. Reference [1] takes into account other restrictions on $\mathcal{R}$ parity violation and estimates that enhancements of the D^0 branching fraction up to the present experimental limit are allowed. This leaves seven orders of magnitude of the D^0 branching fraction to be probed for new physics effects. The current best experimental limit on the $D^0 \to \mu^+\mu^-$branching fraction comes from BELLE [2], and is equal to:

$$\mathcal{B}(D^0 \to \mu^+\mu^-) \leq 1.4 \times 10^{-7} \tag{1}$$

at the 90% confidence level (C.L.). CDF has already performed a search for these rare decays using the first 60 pb^{-1} of Run II data, and set a limit of $\mathcal{B}(D^0 \to \mu^+\mu^-) \leq 2.5 \times 10^{-6}$ [5]. This study builds on the experience of the previous measurement adding more data, using a muon identification likelihood developed for the B_s-mixing analysis, utilizing the CMX subdetector

to increase the coverage of muon identification, and incorporating a more detailed analysis of background sources.

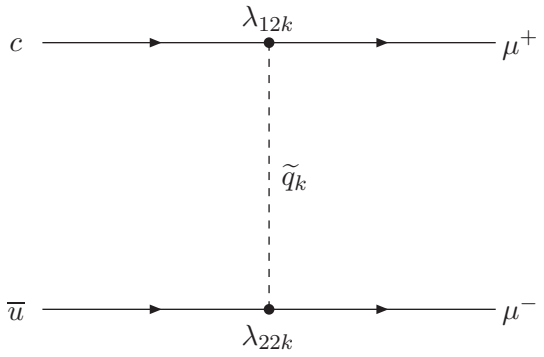

Figure 3: An $\mathcal{R}$-parity violating SUSY $D^0 \to \mu^+\mu^-$ decay process, a possible tree level contribution.

2 Measurement Technique

The strategy of the measurement is rather simple, and follows the same strategy of the previous measurement [5]. Charged, two-body D^0 decays are gathered with the two-track trigger; minimal additional track quality requirements are imposed. The combinatorial backgrounds are vastly reduced by requiring a $D^{*+} \to D^0\pi^+$ tag (or charge conjugate). We demand that the mass difference between the D^{*+} and D^0 candidates fall between 0.144 and 0.147 GeV/c. Figure 4 illustrates the size of the charm sample selected with this technique in the $D^0 \to K^+\pi^-$channel, and the power of the D^* requirement to reduce the background. The resulting $D^0 \to K^+\pi^-$sample of 900,000 decays is used to determine characteristics of the $D^0 \to \mu^+\mu^-$signal.

The two-track candidates are reconstructed with a $\mu^+\mu^-$ mass hypothesis, and the D^* tag mass–difference cut is applied. The mass distributions of the selected events are displayed in Fig. 5. We classify the events according to the muon detector subsystem the tracks intercept, central (CMU) or extension (CMX). Considering both tracks of the D^0 candidate, three cases occur: when both tracks fall in the acceptance of the central muon system the event is classified as CMU-CMU; when both tracks fall in the acceptance of the extension muon system the event is classified as CMX-CMX; and when one track falls in each the event is classified CMU-CMX.

The invariant mass of the track pair is required to fall inside a search window. Using background subtraction, the number of $D^0 \to \mu^+\mu^-$decays in the search window is determined. The $D^0 \to \pi^+\pi^-$peak is used as a reference signal to determine the branching fraction:

$$\mathcal{B}(D^0 \to \mu^+\mu^-) = \frac{N(\mu^+\mu^-)}{N(\pi^+\pi^-)} \cdot \frac{\epsilon(\pi^+\pi^-)}{\epsilon(\mu^+\mu^-)} \cdot \mathcal{B}(D^0 \to \pi^+\pi^-), \tag{2}$$

where $N(\mu^+\mu^-)$ is the number of observed dimuon decays, $N(\pi^+\pi^-)$ is the observed number of reference decays, $\epsilon(\pi^+\pi^-)/\epsilon(\mu^+\mu^-)$ is the relative efficiency for triggering and reconstruct-

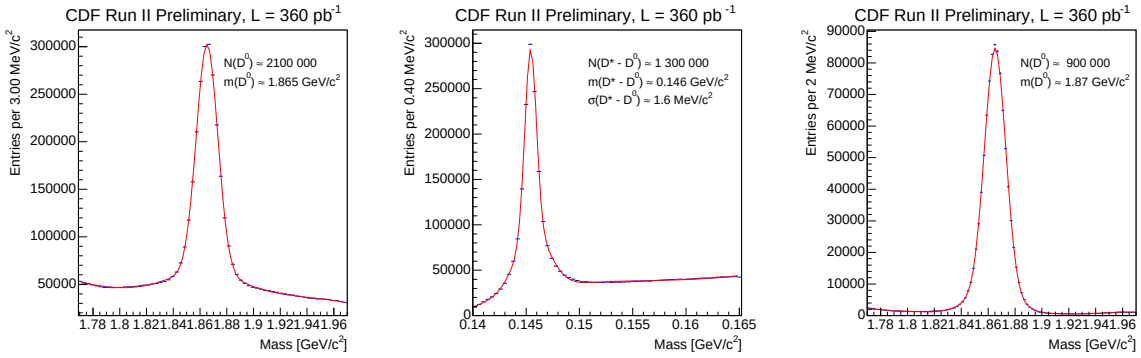

Figure 4: The $D^0 \to K^+\pi^-$reference sample selected with the same basic requirements applied to select the signal. The left plot shows the mass distribution before the D^* requirement. The middle plot shows the difference between the $K\pi\pi$ mass and the $K\pi$ mass used to apply the D^* requirement. And the right plot shows the result of selecting only those decays with a mass difference between 0.144 and 0.147 GeV/c.

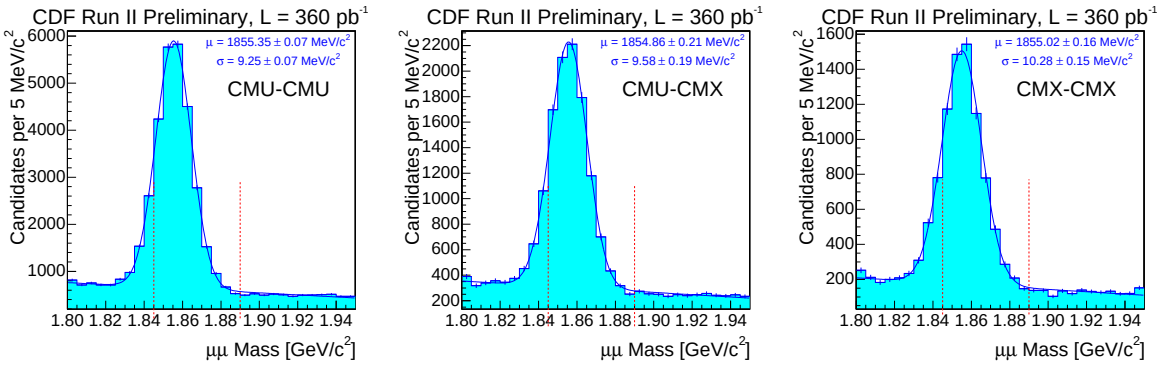

Figure 5: The $\mu^+\mu^-$ mass distributions of events satisfying the basic event selection requirements for CMU-CMU (left), CMU-CMX (middle), and CMX-CMX (right) candidates. The dashed lines indicate the search region for $D^0 \to \mu^+\mu^-$events. The kinematically similar $D^0 \to \pi^+\pi^-$events produce the peak overlapping the search region. These events are used to normalize the $D^0 \to \mu^+\mu^-$measurement, but are also a potential source of background when both pions are misidentified as muons.

ing $\pi^+\pi^-$ and $\mu^+\mu^-$ decays, respectively, and $\mathcal{B}(D^0 \to \pi^+\pi^-) = (1.364 \pm 0.032) \times 10^{-3}$ [3] is the reference branching fraction for $D^0 \to \pi^+\pi^-$ decays.

But $D^0 \to \pi^+\pi^-$decays can also fake the $D^0 \to \mu^+\mu^-$signal if both pions are misidentified as muons. To minimize the misidentification probability we utilize a likelihood function for muon identification that takes into account dE/dx information from the tracker, and electromagnetic and hadronic calorimeter energy deposition, as well as muon detector information. The likelihood function achieves high efficiency while providing additional suppression for hadrons. The probabilities for pions and kaons to be misidentified as muons is estimated from the D^* tagged $D^0 \to K^+\pi^-$data. The results are displayed in Figs. 6–9 as functions of track transverse momentum p_T, pseudorapidity η, and azimuthal angle ϕ.

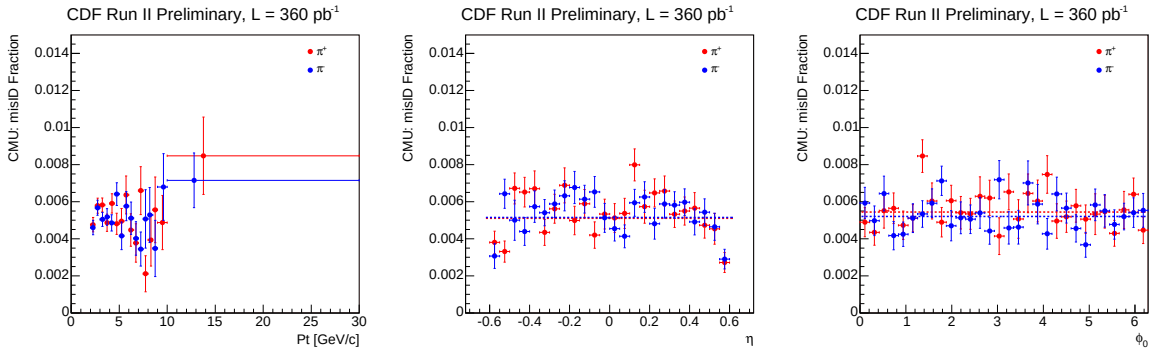

Figure 6: The muon misidentification probabilities for pions in the central muon system as functions of track transverse momentum p_T (left), pseudorapidity η (middle), and azimuthal angle ϕ (right). Positive (red) and negative (blue) pions are shown separately as a cross-check.

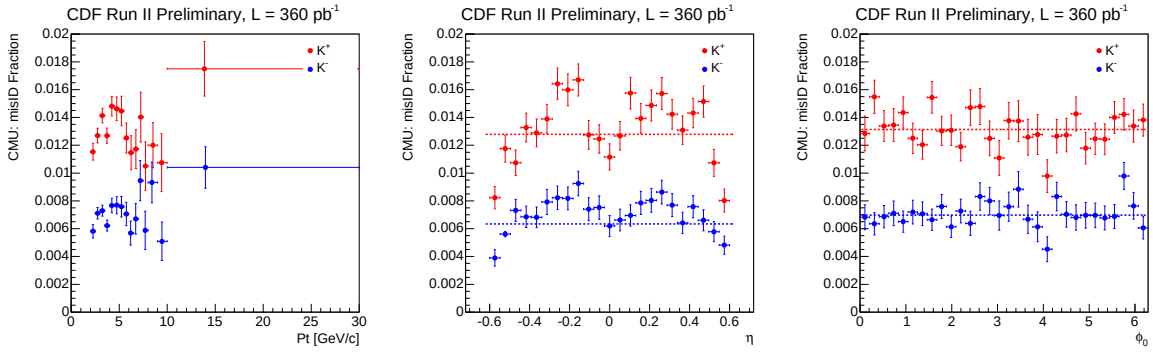

Figure 7: The muon misidentification probabilities for kaons in the central muon system as functions of track transverse momentum p_T (left), pseudorapidity η (middle), and azimuthal angle ϕ (right). Positive (red) and negative (blue) kaons are shown separately as a cross-check.

Different decay processes can mimic $D^0 \to \mu^+\mu^-$decays. The dominant background before muon identification are $D^0 \to \pi^+\pi^-$decays. In addition we consider backgrounds arising

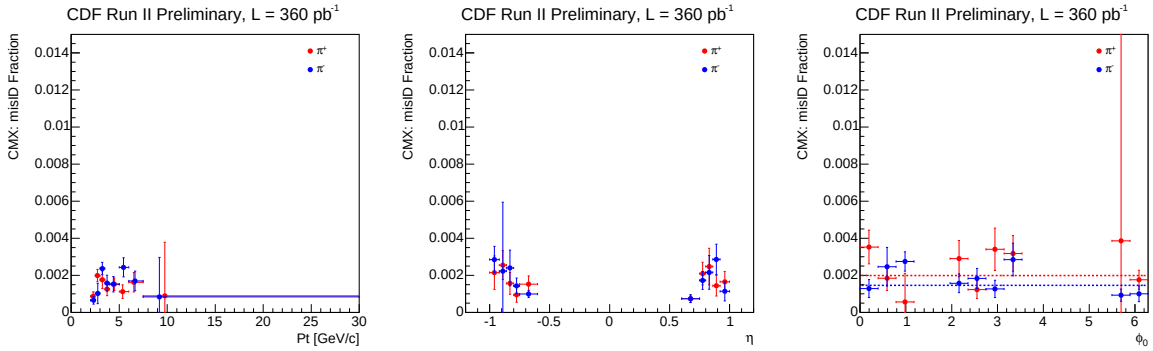

Figure 8: The muon misidentification probabilities for pions in the extension muon system as functions of track transverse momentum p_T (left), pseudorapidity η (middle), and azimuthal angle ϕ (right). Positive (red) and negative (blue) pions are shown separately as a cross-check.

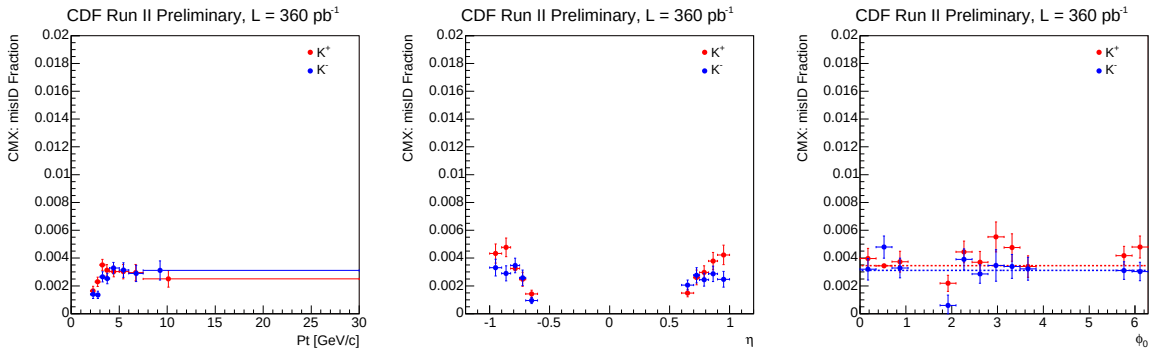

Figure 9: The muon misidentification probabilities for kaons in the extension muon system as functions of track transverse momentum p_T (left), pseudorapidity η (middle), and azimuthal angle ϕ (right). Positive (red) and negative (blue) kaons are shown separately as a cross-check.

from: misidentified $D^0 \to K^+\pi^-$decays; D^* tagged semimuonic D^0 decays with a hadronic track misidentified as a muon; semimuonic b hadron decays with a hadronic track misidentified as a muon; $B \to \mu^+\mu^- X$ decays arising primarily from cascade semimuonic decays of the b hadron and c hadron; and combinatorial background with two misidentified hadrons. Figure fig:bmumu illustrates the sources of background from b hadron decays before muon identification is required, along with the misidentification fractions for the primary contributors.

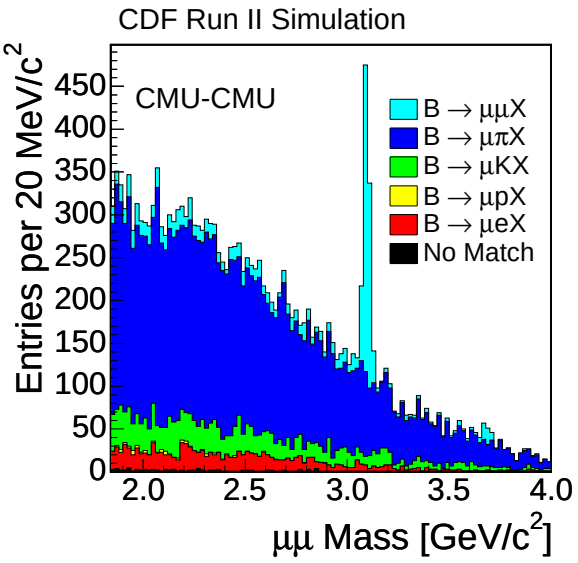

Figure 10: Background sources from B decays.

We find that the main background in the search is due to cascade, semi-muonic B decays, $B \to \mu^-\nu\mu^+\bar{\nu}X$ decays, referred to as $B \to \mu^+\mu^- X$ decays. The measurement is optimized by rejecting the dominant background using a probability ratio discriminating prompt charm from b hadron decays using the impact parameter and displacement significance of the two-track system. Figure 11 demonstrates the discriminating power of these quantities. We find that roughly 85% of the signal can be retained while rejecting about 60% of the dominant background.

Table 1 lists the background contributions to the search window found for each source. The backgrounds are determined separately for each channel. The dominant source is still $B \to \mu^+\mu^- X$ decays. The total background is estimated from the sum in quadrature of all the contributions, where contributions listed as an upper limit are added to the error on the mean, but not the mean itself.

3 Sensitivity and Limits

The interpretation of the measurement is contained in the following equation:

$$\mathcal{B}(D^0 \to \mu\mu) = \frac{N(\mu\mu)}{N(\pi\pi)} \cdot \frac{\epsilon(\pi\pi)}{\epsilon(\mu\mu)} \cdot \mathcal{B}(D^0 \to \pi\pi) \tag{3}$$

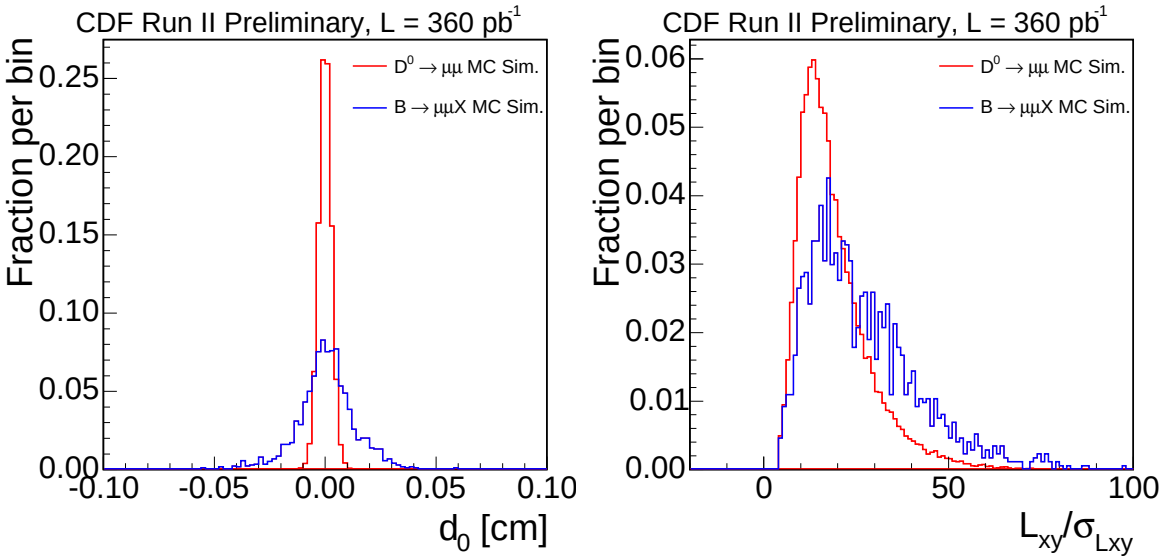

Figure 11: Quantities used to separate prompt charm meson decays from background due to B decays.

Table 1: Background contributions for the optimized analysis selection. Contributions from different sources are summed in quadrature to yield the total estimate. The final row is the number of observed decays in the search window for each channel.

Source	CMU-CMU	CMU-CMX	CMX-CMX
Combinatorial Background	0.040 ± 0.007	0.008 ± 0.001	0.0007 ± 0.0001
$D^0 \to \pi\pi$ double fakes	0.53 ± 0.005	0.057 ± 0.001	0.012 ± 0.002
$D^0 \to K\pi$ double fakes	< 0.01	< 0.01	< 0.01
Semimuonic D^0 decays	< 0.36	< 0.20	< 0.10
Semimuonic B Decays	0.54 ± 0.06	0.13 ± 0.03	0.07 ± 0.02
Cascade semimuonic B decays	3.8 ± 1.3	2.5 ± 1.0	1.0 ± 0.5
Total	4.9 ± 1.3	2.7 ± 1.0	1.0 ± 0.5
N_{obs}	3	0	1

where $N(\mu\mu)$ is the observed number of $D^0 \to \mu\mu$ decays in the search window, $N(\pi\pi)$ is number of reference $D^0 \to \pi\pi$ decays, $\epsilon(\mu\mu)$ and $\epsilon(\pi\pi)$ are the efficiencies for accepting di-muon and di-pion decays, respectively, and $\mathcal{B}(D^0 \to \pi\pi)$ is the branching fraction for the reference $D^0 \to \pi\pi$ decay. The number of observed $D^0 \to \mu\mu$ decays is calculated by subtracting the number of expected decays due to background processes, $N_{\rm bkg}$ from the number of observed decays in the search window, $N_{\rm obs}$:

$$N(\mu\mu) = N_{\rm obs} - N_{\rm bkg}. \tag{4}$$

If a significant excess of observed decays over expected decays is found, the interpretation of the result is trivial. The number of $D^0 \to \mu\mu$ decays is calculated from Eq. 4, and the observed branching fraction is calculated from Eq. 3.

The question is slightly more complicated in the case of setting limits, mostly because a lot of the inputs to Eqs. 3 and 4 have uncertainties. For instance, the efficiencies $\epsilon(\mu\mu)$, $\epsilon(\pi\pi)$, the number of expected decays $N_{\rm bkg}$ are all measured quantities with associated uncertainties which have to be taken into account when setting limits. Obviously, one also wants to combine the results obtained in the three channels: CMU-CMU, CMU-CMX and CMX-CMX. We use a hybrid frequentist/Bayesian approach to setting limits on $\mathcal{B}(D^0 \to \mu^+\mu^-)$ that allows for the combination of a number of channels and the inclusion of uncertainties on input quantities (nuisance parameters) [7]. As a cross check, we use a purely Bayesian approach that allows for the combination of a number of channels and the inclusion of uncertainties on input quantities (nuisance parameters) [8].

The sensitivity of the measurement was estimated using the estimated efficiencies and backgrounds, and assuming zero signal. We generate 1000 "toy experiments", each with a number of events observed randomly generated according to a poisson distribution with mean equal to the expected background. The limit on the branching ratio is calculated at the 90%, and 95% confidence level. The distributions of limits are displayed in Figs. 12–13. The median of the distribution of limits is quoted as the sensitivity of the measurement. The senstivity for limits is 5.2×10^{-7} (6.0×10^{-7}) at the 90% (95%) confidence level and is indicated by the green arrows in Figs. 12–13.

The sensitivity was estimated for the purely Bayesian approach used to cross check the results. We generate 1000 "toy experiments", each with a number of events observed randomly generated according to a poisson distribution with mean equal to the expected background. The limit on the branching ratio is calculated at the 90%, and 95% credibility level. The distributions of limits are displayed in Figs. 14–15. The median of the distribution of limits is quoted as the sensitivity of the measurement. The sensitivities are 6.5×10^{-7} at the 90% credibility level, and 7.8×10^{-7} at the 95% credibility level and are indicated by the blue arrows in Figs. 14–15.

We count the number of events found in the signal mass window, shown in Fig. 16. We find three candidates in the CMU-CMU channel, none in the CMU-CMX channel and one candidate in the CMX-CMX channel, listed in the last row of Table 1. These observations are consistent with expected background, so we will quote a limit on the branching fraction.

The resulting limit is

$$\mathcal{B}(D^0 \to \mu^+\mu^-) < 2.1 \times 10^{-7} \text{ at the } 90\% \text{ C.L.}$$

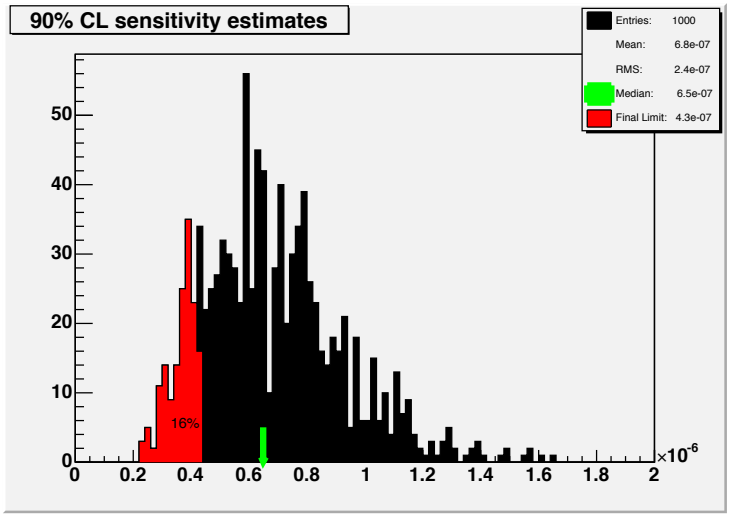

Figure 12: The distribution of limits at the 90% confidence level obtained. The median of the distribution is indicated by the green arrow. The red shaded area indicates those results equal to or less than the result obtained for our data.

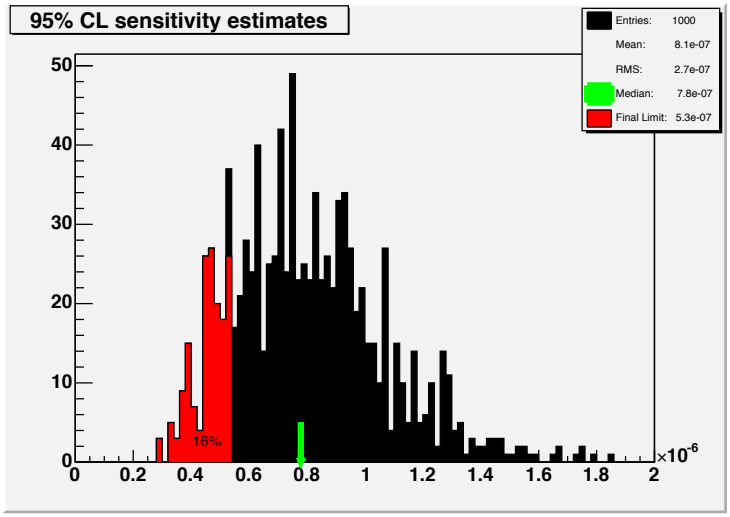

Figure 13: The distribution of limits at the 95% confidence level obtained. The median of the distribution is indicated by the green arrow. The red shaded area indicates those results equal to or less than the result obtained for our data.

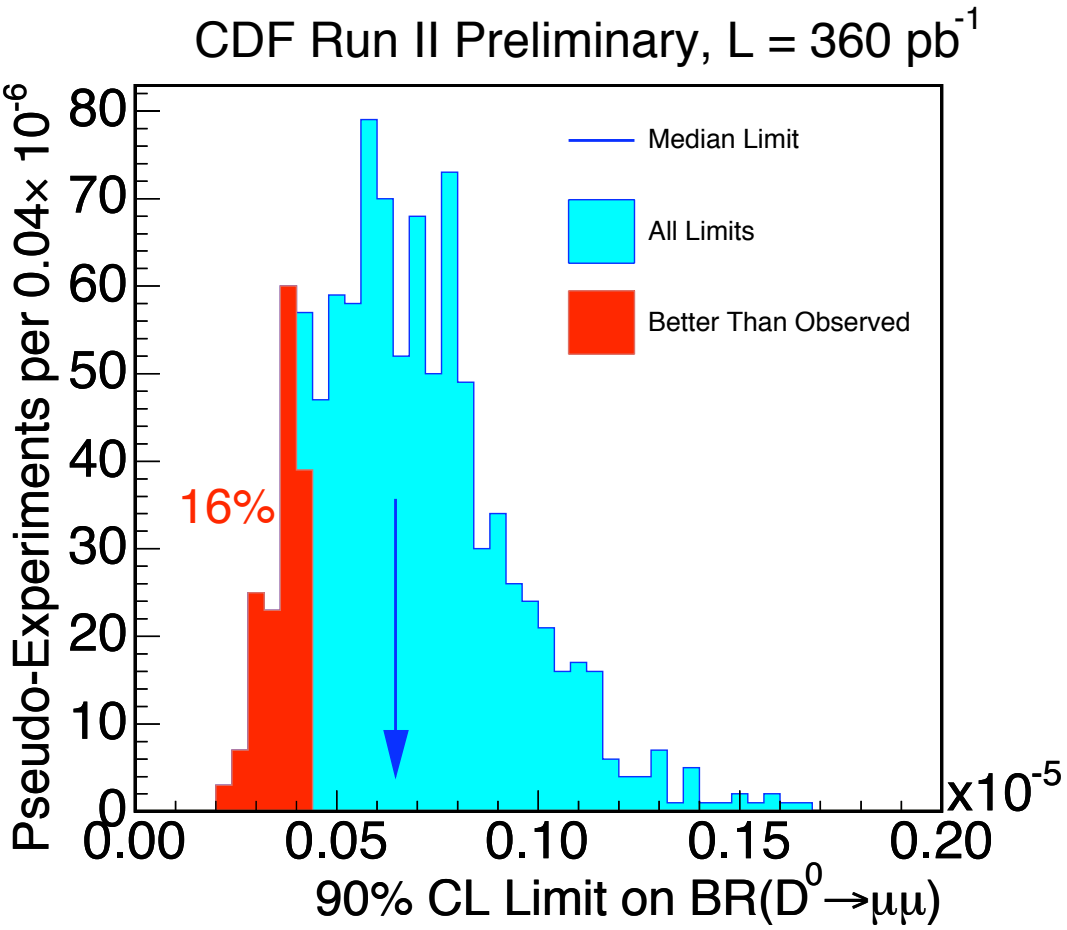

Figure 14: The distribution of limits at the 90% credibility level obtained for 1000 toy experiments. The median of the distribution is indicated by the blue arrow. The red shaded area indicates those results equal to or less than the result obtained for our data.

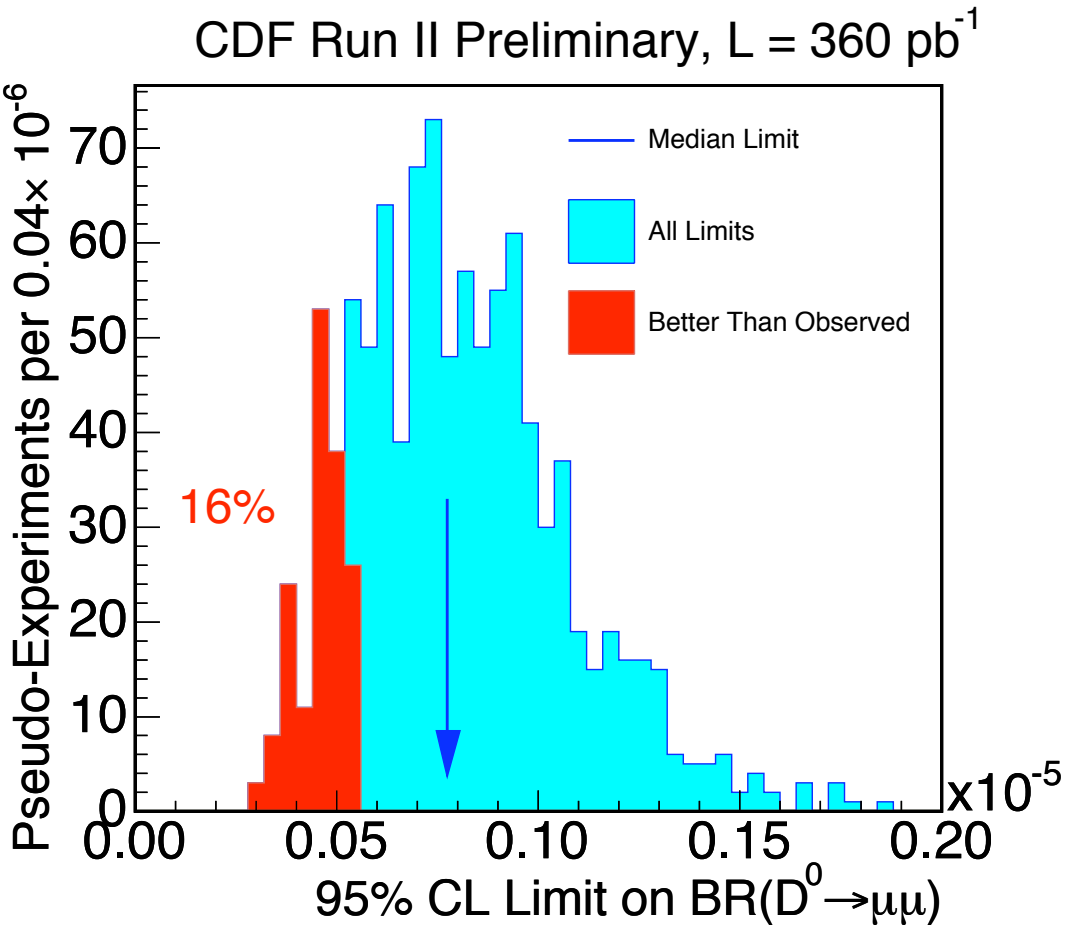

Figure 15: The distribution of limits at the 95% credibility level obtained for 1000 toy experiments. The median of the distribution is indicated by the blue arrow. The red shaded area indicates those results equal to or less than the result obtained for our data.

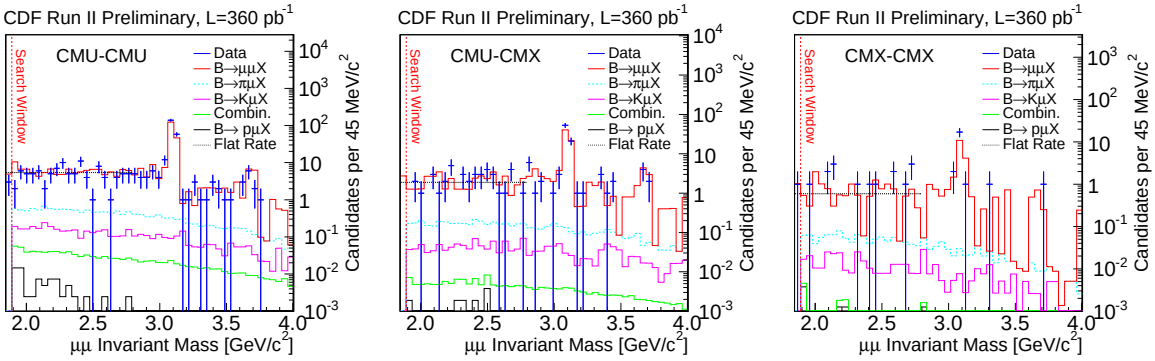

Figure 16: The distributions of $\mu^+\mu^-$ mass in a wide window above the D^0 mass for data (blue crosses) and the background model after all analysis requirements have been applied. The background model histograms are stacked; the red histogram indicates the total of the background model and shows very good agreement with the data. The three plots are for the CMU-CMU (left), CMU-CMX (center), and CMX-CMX (right) subsamples. The $D^0 \to \mu^+\mu^-$search window is the single, leftmost bin of each plot.

and

$$\mathcal{B}(D^0 \to \mu^+\mu^-) < 3.0 \times 10^{-7} \text{ at the } 95\% \text{ C.L.}$$

The probability for these limits, assuming there is really no signal, is about 16% and is indicated in Figs. 12 and 13.

The purely Bayesian calculation yields

$$\mathcal{B}(D^0 \to \mu^+\mu^-) < 4.3 \times 10^{-7} \ (5.3 \times 10^{-7})$$

at the 90% (95%) credibility level.

4 Conclusions

We have presented an update of the search for FCNC $D^0 \to \mu^+\mu^-$ decays using 360 pb^{-1} of Run II data. The analysis has been expanded to also include muons in the fiducial region of the CMX detector. The increased sample size allows for a more detailed study of the dominant background, resulting in a first identification of $B \to \mu\mu X$ decays as being the most likely physics source of background in the signal mass range. Using a likelihood ratio function, we reject about half of the dominant background while keeping almost 85% of the signal. After looking at events in the signal region, we find 3 CMU-CMU, 0 CMU-CMX and 1 CMX-CMX candidates. We set the following limits on the branching ratio of the D^0 decay: $\mathcal{B}(D^0 \to \mu^+\mu^-) < 2.1 \times 10^{-7}$ at the 90% CL, and $\mathcal{B}(D^0 \to \mu^+\mu^-) < 3.0 \times 10^{-7}$ at the 95% CL. This is roughly 50% looser than the best published result [2], and an improvement of roughly a factor of ten with respect to the previous CDF analysis [5].

References

[1] G. Burdman, E. Golowich, J. Hewett, S. Paskvasa, "Rare Charm Decays in the Standard Model and Beyond", `arXiv:hep-ph/0112235` v2 (March 2002)

[2] M. Petrič *et al.* (Belle Collaboration), Phys. Rev. D **81**, 091102R (2010).

[3] W.-M. Yao *et al.*, Journal of Physics G **33**, 1 (2006).

[4] E. Berry, I.K. Furic, "Study of Muon Matching Efficiencies and Mistag Rates", CDF Note 8042 (2006).

[5] W.J. Ashmanskas and R. Harr., "Search for the FCNC decay $D^0 \to \mu^+\mu^-$using the hadronic B trigger", CDF Note 6723 (2003).

[6] K. Bloom and D. Dagenhart., "Muon-Reconstruction Efficiency", CDF Note 6029 (2002).

[7] E. Berry, I.K. Furĭc, R. Harr, and Y.K. Kim, "Frequentist Limit for $D^0 \to \mu^+\mu^-$Analysis", CDF Note 9501 (2008).

[8] J. Heinrich, "Bayesian limit software; multi-channel with correlated backgrounds and efficiencies", CDF Note 7587 (2005).